PAPER

Check for updates

Insight into the hetero-interactions of 4-nonylphenol with dissolved organic matter: multiple spectroscopic methods, ^{1}H NMR study and principal component analysis†

Rui Gao, [ID] Hao Wang, Abliz Abdurahman, Weiqian Liang, Xiaotian Lu, Shuyin Wei and Feng Zeng [ID] *

Understanding the interactions between heterogeneous dissolved organic matter (DOM) and nonylphenols (NPs) is essential for predicting their behavior and fate in the environment. Herein, we firstly obtained different MW-fractionated humic acids (HAs) using the ultrafiltration method. Afterward, the molecular weight (MW)-dependent interactions of HAs with 4-nonylphenol (4-NP) were analysed by excitation emission matrix (EEM) fluorescence spectroscopy, fluorescence quenching, UV-vis spectroscopy, Fourier transform infrared (FT-IR) spectroscopy, nuclear magnetic resonance (NMR) spectroscopy and principal component analysis (PCA). EEM spectra indicated that the quenching mechanism was static. In the binding process, the higher MW fractions showed stronger interaction with 4-NP than the lower MW counterparts, exhibiting a clear MW-dependent interaction heterogeneity. The interaction constants for the 4-NP–HAs system were suppressed as the ionic strength decreased and pH increased, which was especially obvious in the binding of 4-NP to the lower MW-fractionated HAs. The FTIR spectra revealed that hydroxyl and aromatics were involved in the interaction process of HA fractions with 4-NP. It was also found from ^{1}H NMR that $\pi-\pi$ interactions between aromatic rings of 4-NP and MW-fractionated HAs were responsible for the complexation. The correlation analysis and PCA results indicated that aromaticity and MW play important roles in the interaction process and confirmed an obvious interaction heterogeneity among MW-fractionated HAs samples. This work highlighted MW-dependent interaction heterogeneities of HA, which suggested that heterogeneity in MW distribution should be taken into consideration when exploring the fate and biogeochemistry cycling of 4-NP from contaminated environments.

1. Introduction

Nonylphenol ethoxylates (NPEOs), as one of the crucial classes of nonionic surfactants, are widely used in agricultural, domestic, and industrial fields.[1] As a result of chemical and biological processes, NPEOs can be degraded stepwise by losing ethoxylates to form more toxic nonylphenols (NPs).[2] Nowadays, NPs have been broadly detected in various environmental matrices, including water, soil, and atmosphere.[1,3–5] They were found to mimic the natural hormone oestrogen, resulting in disrupting the normal functioning of the hormonal system. Due to these disturbing results, NPs were designated as priority hazardous substances in European Union.[6] Currently, investigating the occurrence, fate, and potential ecological risks of NPs

in the aquatic, terrestrial, and atmospheric environments is urgent.[1,3–5]

Due to the nonyl chain, NPs have hydrophobic properties.[4] The highly hydrophobic NPs pose a strong intendancy to interaction with soil/sediment organic matter, especially the ubiquitous dissolved organic matter (DOM), which significantly influence the transportation, transformation, and bioavailability of NPs in the environments.[7–10] By using dialysis equilibrium experiments, Li et al.[10] found DOM had high affinity to adsorb NPs. Liao et al.[8] investigated the kinetics and thermodynamics of NP sorption to the DOM, and the results indicated that the pseudo first order model and Freundlich model could better describe the sorption process. Because of the interactions between DOM and NPs, the adsorption of NPs was inhibited by magnetic reduced graphene oxides. Unfortunately, DOM is a well-known heterogeneous mixture in the environment. However, till now, the previous works about 4-NP–HA interaction mainly focused on the bulk HA samples, ignoring the

School of Chemistry, Sun Yat-sen University, Guangzhou, Guangdong, 510275, China. E-mail: ceszf@mail.sysu.edu.cn

effects of the heterogeneities within the bulk HA on the environmental behaviors.

DOM is a complex and heterogeneous mixture of organic macromolecules consisting of different sizes, structures, and chemical properties.[11,12] The interactions between pollutants with DOM molecules were significantly related to the organic compound species and MW distribution. For example, some studies revealed that high molecular weight MW-fractionated HAs which exhibited higher aromaticity and hydrophobicity had superior sorption ability on the other hydrophobic organic compounds (HOCs).[12–15] Nevertheless, recent researches observed that lower molecular weight MW-fractionated DOM (<1 kDa) had strong adsorption affinities on bisphenol A, octylphenol and pentachlorobenzene.[16,17] This discrepancy may be attributed to the composition heterogeneity of DOM and non-uniformity of HOCs binding functionalities in DOM. Therefore, understanding the interactions between different MW DOM and NPs under different environmental conditions, particularly the underlying interaction mechanisms, is imperative.

The interaction of HOCs with DOM has been investigated using various techniques, such as dialysis equilibrium, passive dosing, solubility enhancement, and fluorescence quenching.[18–21] Among them, fluorescence quenching is a popular and powerful method due to its sensitivity, non-destructivity, and simplicity.[22] It has been reported as an efficient method to investigate the interaction mechanism between HOCs and fluorescent substances.[11,16,20] However, the binding sites are easily overlooked when exploring interactions.[20] Nuclear magnetic resonance (NMR) can be used to provide specific, molecular-level information involved in the interaction, and it is also applied to investigate those occurring between environmental pollutants and DOM.[23,24] Additionally, principal component analysis (PCA) is a multivariate statistical technique that can obtain the main comprehensive influencing factors of interactions. However, limited information has been probed into the interaction mechanism between DOM and multi-antibiotic situations. Therefore, combining these techniques can better understand the interaction mechanism between DOM and NPs deeply regarding binding capacities and binding sites.

The aim of this paper was to provide insights into the hetero-interactions of NP with DOM in the natural environment. To achieve this purpose, 4-nonylphenol (4-NP) and a soil HA, were selected as the representative NP and DOM, respectively. We utilized the ultrafiltration technique was applied to fractionate the HA samples into different MW-fractionated HAs. Furthermore, the interaction properties between MW-fractionated HAs and 4-NP were investigated at different temperatures/pHs/ionic strengths by fluorescence quenching method. UV-visible spectroscopy and FTIR spectroscopy were introduced to further explore the internal mechanism of the interaction of 4-NP with MW-fractionated HAs. The possible interaction sites were discussed by ^{1}H NMR analysis. The correlation analysis and principal component analysis were performed to understand the hetero-interaction. The results provide new insights into the binding interactions of the MW-dependent interaction

heterogeneities of HA with 4-NP, which can improve our understanding of the fate and bioavailability of HOCs in aquatic environments.

2. Experimental

2.1. Materials

4-NP (>99.5%), NaOD, DMSO-D$_6$ and D$_2$O were purchased from Sigma-Aldrich. Physicochemical properties of 4-NP were listed in Table S1.† According to the method of the International Humic Substances Society (IHSS), HA was extracted from soil samples, collected from an undisturbed area at Dunhua, Jilin Province, China (43°18′36″N, 128°23′26″E). Amicon Ultra-15 centrifugal filters with nominal molecular weight cut-off of 3 kDa, 10 kDa, 30 kDa, and 100 kDa were obtained from Millipore (Darmstadt, Germany). The other reagents were purchased from Guangzhou Chemical Reagent (Guangzhou, China). If not specified, all the reagents were used as received without further purification. Ultrapure water (18.2 Ω cm^{-1}, purification by a Millipore system) was used throughout the experiments.

2.2. Fractionation and characterization of HA

The stock solution of HA was stirred overnight, followed by filtering through a 0.22 μm cellulose acetate filter paper (Millipore, Billerica, MA, USA). The filtrate was referred to as pristine HA. The HA fractions were obtained by using the Amicon Ultra-15 centrifugal filters and the detailed fractionation procedures were given elsewhere.[25] The fractions achieved were named >100 kDa HA, 30–100 kDa HA, 10–30 kDa HA, 3–10 kDa HA, and <3 kDa HA. Concentrations of pristine and MW-fraction HAs were quantified using a total organic carbon (TOC) analyzer (TOC-VCPH, Shimadzu, Japan). The pristine- and MW-fractionated HAs were stored in the dark at 4 °C until use. The MW distribution, elemental compositions, UV-visible absorption spectra, size exclusion chromatography (SEC), and excitation–emission matrices (EEM) fluorescence spectra of pristine- and MW-fractionated HAs were characterized and the results were are given in the ESI.†

2.3. Fluorescence quenching experiments

The interaction properties of pristine and MW-fractionated HAs with 4-NP were examined by using the fluorescence quenching method. Batch interaction experiments were conducted using several glass vials filled with MW-fractionated HA, then the 4-NP stock solution was spiked into the HA solutions. The corresponding electrolyte solution was added to each vial to maintain a final volume of 10 mL, HAs at 0.5–10 mg C L^{-1} and 4-NP at 1 mg L^{-1}. The pH was adjusted using HNO$_3$ or NaOH. The IS was modified by adding NaNO$_3$. After mixing, the vials were gently shaken by an oscillator for 4 h at 288 K, 298 K, and 308 K. This time period was adequate for reaction equilibrium based on preliminary experiments. After the equilibrium period, UV-visible absorbance spectra and EEM fluorescence spectra were measured.

2.4. Spectral measurement

The UV-visible absorbance spectra were measured between 200 and 800 nm using a spectrophotometer (UV-2550, Shimadzu, Japan) with 1 cm quartz cells. If not specified, the concentration of HAs was 5 mg C L^{-1}. To get better FTIR spectra of 4-NP, HAs, and their complexes, the high concentration solutions of samples were prepared and freeze-dried. And all the obtained particles were homogenized and pressed under the irradiation of an infrared lamp to eliminate the effect of moisture in the samples. The FTIR spectra were recorded in a PerkinElmer frontier spectrometer equipped with a Germanium attenuated total reflection accessory and a KBr beam splitter with 32 scans at a resolution of 4 cm^{-1}. All ^{1}H NMR spectra data were collected on a Bruker Avance 400 MHz instrument at 400.13 MHz with a 5 mm Bruker inverse broadband probe. The temperature was set as 298 ± 1 K. Typically, 1 mg 4-NP was firstly added with 50 μL DMSO-D$_6$ to ensure 4-NP dissolution, and then diluted in 0.1 mol L^{-1} NaOD solution with the final concentration of 120 μg mL^{-1}, and then the solid pristine and MW-fractionated HAs were added, respectively. The concentration ratio of HA with 4-NP in all samples was 0.5. The alkaline conditions were favorable for the dissolution of 4-NP and HAs. The resulting solution was sonicated for 120 s and transferred to NMR tubes. High concentrations of HAs and 4-NP were used to enhance the intensity of ^{1}H NMR and thus improve the signal-to-noise ratio of the analysis. ^{1}H NMR spectra were referenced to the chemical shift of the solvent being 4.709 ppm. All spectra were processed by MestReNova software. All samples were performed in triplicate and the results in average were reported.

2.5. Data analysis

All fluorescence spectra were corrected for the inner filter effect as follows:[26]

$$F = F_{obs}\text{anti}\log\left(\frac{A_{ex} + A_{em}}{2}\right) \tag{1}$$

where F_{obs} and F were the fluorescence intensities before and after correction, and A_{ex} and A_{em} were the absorbance of the test solution at excitation and emission wavelengths, respectively.

The interaction parameters of 4-NP to the pristine and MW-fractionated HAs were calculated using the Stern–Volmer equation:[20]

$$\frac{F_0}{F} = 1 + k_q\tau_0[\text{HA}] = 1 + K_{HA}[\text{HA}] \tag{2}$$

where F_0 and F were the corrected fluorescence intensities of 4-NP without and with pristine and MW-fractionated HAs. k_q was the energy transfer rate (L mol^{-1} s^{-1}), τ_0 was the lifetime of fluorescence (3.63 ns),[27] [HA] was the added concentration of HA and K_{HA} was the sorption coefficient. Because the HA fraction possessed intrinsic fluorescence at excitation wavelength of 4-NP. In order to remove background effects, a blank was made for each concentration of HA fraction. The blank spectrum was subtracted from the emission spectrum of the corresponding 4-NP–HA solution.[20]

In addition, the interaction constant (K) and the number of interaction sites (n) according to fluorescence titration experiments were calculated from the site-binding equation for an interaction process involving a static quenching mechanism:[28]

$$\log\frac{F_0 - F}{F} = \log K + n\log[\text{HA}] \tag{3}$$

where F_0 and F were the corrected fluorescence intensities of 4-NP in the absence and presence of pristine and MW-fractionated HAs. [HA] was the added concentration of HA (mg C L^{-1}). The thermodynamic parameters for fluorescence quenching of 4-NP by HAs, including the enthalpy change (ΔH), the entropy change (ΔS), and the Gibbs free energy change (ΔG), were used to interpret the interaction forces. The values of ΔH and ΔS can be estimated from eqn (4):

$$\log K = -\frac{\Delta H}{RT} + \frac{\Delta S}{R} \tag{4}$$

where R was the ideal gas constant (8.314 J mol^{-1} K^{-1}), T was the absolute temperature and K was the interaction constant at temperature T. Then the ΔG could be determined using the following eq:

$$\Delta G = \Delta H - T\Delta S \tag{5}$$

Details of the data analysis for the interaction of pristine and MW-fractionated HAs with 4-NP were given in the ESI.†

3. Results and discussion

3.1. Physicochemical properties of the pristine and MW-fractionated HAs

Separated by ultrafiltration, the MW-fractionated HAs showed apparent increases in molecular weights ranging from 2.30 to 20.9 kDa (Fig. S1 and Table S2†). Elemental compositions and atomic ratios of the pristine and MW-fractionated HAs were listed in Table S2.† With the enhancement of molecular weights of the MW-fractionated HAs, an increasing and a decreasing trend was observed for the H/C ratios and the O/C ratios, respectively, indicated that the high molecular weight MW-fractionated HAs contained more unsaturated hydrocarbons
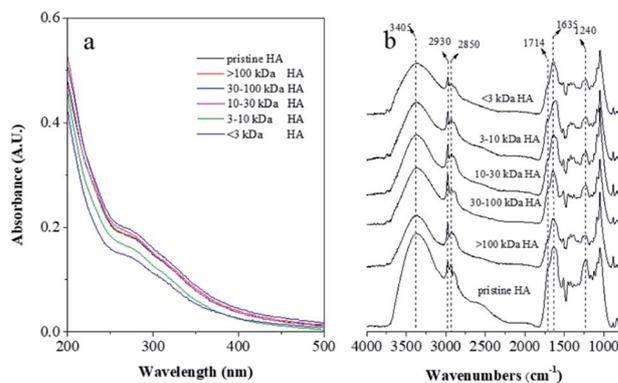

Fig. 1 UV-visible absorption (a) and ATR-FTIR (b) spectra of pristine- and MW-fractionated HAs.

and less oxygen-containing functional groups.[29–31] Fig. 1a shows that UV-visible absorbance of the pristine and MW-fractionated HAs decreased monotonously as the wavelength increased and no absorption peak was observed. Except for 30–100 kDa HA, SUVA$_{254}$ values of molecular weight MW-fractionated HAs which were calculated via the division of the absorbance at 254 nm with TOC concentration, decreased from 9.24 to 6.99 with decreasing molecular weight of the MW-fractionated HAs. Polarity which defined as the elemental ratio of (O + N)/C increased from 0.51 for >100 kDa HA to 0.65 for <3 kDa HA. These results indicated that the higher molecular weight MW-fractionated HAs (>30 kDa HA) contained more aromatic compounds and hydrophobic structures.[29,32,33]

As presented in Fig. 1b, with decreasing molecular weight of the MW-fractionated HA, the absorbances of peaks at 3405, 1714 and 1240 cm^{-1} were increased slightly, corresponding to the O–H stretching of carboxyl acids, phenols and alcohol, C=O stretching of carboxylic acid, aldehyde and ketone, and C–O stretching of ester, ethers and phenols, respectively,[30] suggesting that the lower molecular weight MW-fractionated HA contained more carboxyl groups, consistent with the elemental analysis.

One fluorescence peak (Ex/Em, Ex: 280–305 nm; Em: 435–474 nm) in each sample was observed (Fig. 2), indicating that the fluorophore was the humic acid-like structure.[21] Generally, the greater abundance of aromatic chromophore possessed, the more red-shift of Em maxima was observed.[29,34] As the molecular weight of the MW-fractionated HAs increased, the peak Em wavelengths shifted towards the longer wavelengths, which suggested more condensed and polymerized structures in higher molecular weight counterparts. Furthermore, the fluorescence intensity of HA was positively related with the content of electron donating groups, such as hydroxyl and methoxyl groups.[35–37] These groups could improve the fluorescence of DOM by increasing the transition probability between the singlet and the ground state. In our study, the fluorescence intensity of the MW-fractionated HAs decreased with the increased molecular weight. The result may contribute to the low content of the oxygen-containing functional groups in HA fractions of higher molecular weight.[35–37] Similar findings have also been reported in the MW-fractionation of DOM.[29,32,33,37]
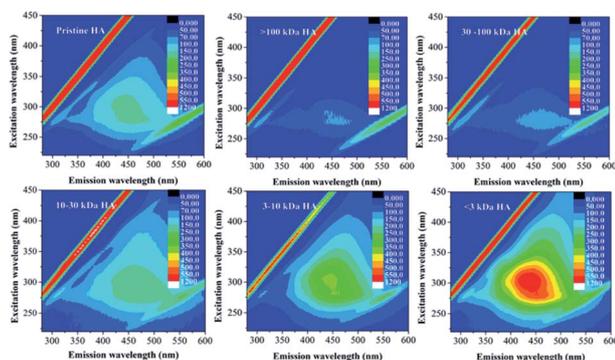
Humification index (HIX) was positively related to the MW of the fractions (except for >100 kDa HA), indicating that the extent of humification decreased with decreasing molecular weight.[33]

3.2. Hetero-interaction of 4-NP with MW-fractionated HAs via an EEM fluorescence spectral analysis

3.2.1. Fluorescence quenching spectra. Fluorescence quenching is a popular and powerful method due to its sensitivity, non-destructivity, and simplicity.[22] It occurs when a fluorescent component interacts with a quencher, the fluorescence intensity of the component weakens or disappears. Fig. 3 and S2† showed the fluorescence quenching of 4-NP by different concentrations of pristine and MW-fractionated HAs. The 4-NP presented a high fluorescence intensity at Ex/Em = 280/308 nm. The fluorescence intensity of the peak was gradually reduced with increasing HAs concentrations due to the suppression of energy emission.[38] At an identical HA concentration, the reduction of the fluorescence intensity was correlated with the molecular weight of the HAs, indicating a strong fluorescence quenching effect of the high molecular weight of MW-fractionated HAs on 4-NP (Fig. S3†).

Generally, fluorescence quenching includes dynamic and static quenching. In order to confirm the quenching mechanism, the Stern–Volmer model was utilized and the exponential curves were presented in Fig. S4.† It can be seen that all the titration data were well fitted with the Stern–Volmer equation ($R^2 = 0.995$–0.999), and the highly linear plot indicated a sole dynamic or static quenching process was responsible for the fluorescence quenching of 4-NP by the HAs.[38,39] The quenching constant of K_q for pristine and MW-fractionated HAs were significantly larger than the maximum scatter collision quenching constant reported for dynamic quenching (2.0 × 10^{10} L mol^{-1} s^{-1}),[27] indicating that static quenching dominated the quenching process and a ground-state complex formed

Fig. 2 The fluorescence EEM spectra of the 5 mg C L^{-1} pristine- and MW-fractionated HAs.

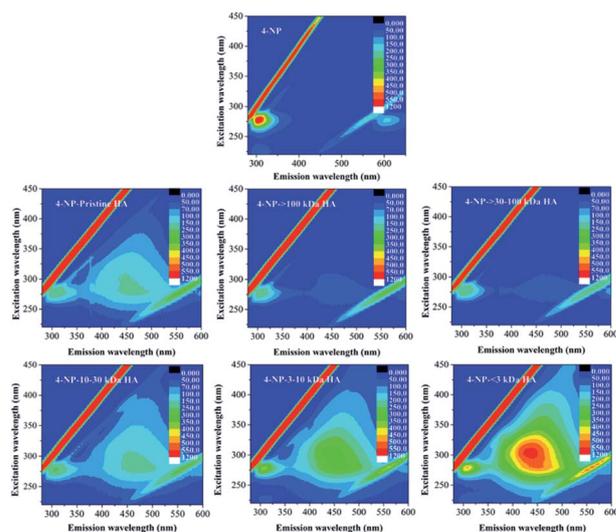**Fig. 3** The fluorescence EEM spectra of 4-NP in the absence and presence of 5 mg C L^{-1} pristine- and MW-fractionated HAs; T = 298 K; pH = 6.0, 1 mol L^{-1} NaNO$_3$.

Table 1 Binding parameters and thermodynamic parameters of 4-NP–HAs systems based on the fluorescence titration experiments (pH 6.0, 1 mmol L^{-1} NaNO$_3$)

		Stern–Volmer equation				Site binding equation					
HAs	T (K)	K_q (L mol^{-1} s^{-1})	K_{HA} (L (mg C)$^{-1}$)	log K_{HA} (L (kg C)$^{-1}$)	R^2	K (L (mg C)$^{-1}$)	n	R^2	ΔG (kJ mol^{-1})	ΔH (kJ mol^{-1})	ΔS (J mol^{-1} K^{-1})
Pristine HA	288	3.40×10^{14}	0.119	5.07	0.999	0.124	0.978	0.995	−16.2	27.1	150
	298	3.07×10^{14}	0.139	5.14	0.999	0.132	1.02	0.995	−17.8		
	308	2.58×10^{14}	0.154	5.18	0.999	0.136	1.06	0.998	−19.2		
>100 kDa HA	288	4.34×10^{14}	0.126	5.10	0.999	0.138	0.952	0.984	−16.7	27.9	155
	298	4.03×10^{14}	0.145	5.16	0.999	0.142	1.01	0.993	−18.4		
	308	3.40×10^{14}	0.155	5.19	0.998	0.144	1.06	0.998	−19.8		
30–100 kDa HA	288	1.55×10^{14}	0.115	5.06	0.999	0.116	0.968	0.989	−14.4	24.6	130
	298	1.42×10^{14}	0.134	5.13	0.999	0.130	1.01	0.994	−15.7		
	308	1.22×10^{14}	0.147	5.17	0.999	0.133	1.05	0.997	−17.1		
10–30 kDa HA	288	8.03×10^{13}	0.109	5.04	0.999	0.099	0.985	0.978	−12.9	25.6	133
	298	7.22×10^{13}	0.124	5.09	0.999	0.119	1.01	0.983	−13.9		
	308	6.36×10^{13}	0.138	5.14	0.996	0.117	1.07	0.995	−15.6		
3–10 kDa HA	288	4.53×10^{13}	0.083	4.92	0.999	0.094	0.985	0.976	−10.5	22.1	113
	298	3.96×10^{13}	0.091	4.96	0.999	0.097	0.955	0.994	−11.6		
	308	3.61×10^{13}	0.104	5.02	0.995	0.107	0.980	0.998	−12.8		
<3 kDa HA	288	2.42×10^{13}	0.053	4.73	0.999	0.061	0.934	0.997	−8.99	20.3	102
	298	2.08×10^{13}	0.065	4.81	0.999	0.072	0.957	0.999	−10.2		
	308	1.69×10^{13}	0.076	4.88	0.998	0.081	0.969	0.999	−11.0		

between HAs and 4-NP. For an interaction involving static quenching mechanism, the site-binding equation was applied to determine the K and n. As listed in Table 1, the log K_{HA} of the MW-fractionated HAs decreased as the molecular weight of the MW-fractionated HAs decreased, displaying a clear MW-dependent interaction heterogeneity. The results indicated the higher interaction affinities for the high molecular weight MW-fractionated HA.[12–15,40] The values of n were approximately 1, suggesting a single binding site in 4-NP for MW-fractionated HAs, which was similar to the previous studies of disinfection byproducts-human serum albumin binary systems[41] and antibiotics-HA.[20]

3.2.2. Thermodynamic parameters. In order to interpret the possible interaction forces between 4-NP and HAs, the interaction of HAs to 4-NP at different temperatures were performed and the corresponding thermodynamic parameters, including ΔH, ΔS, and ΔG were calculated. As listed in Table 1, the K and K_{HA} values MW-fractionated HAs also exhibited similar trends, which were decreased with the molecular weight of HAs decreasing. K and K_{HA} increased with increasing temperature for all HAs, suggesting that the interaction properties of 4-NP for MW-fractionated HAs became stronger with increasing temperature. As we know, dynamic quenching is enhanced by increasing temperature, whereas decreasing temperature most likely causes higher static quenching constants. The temperature-dependent results further demonstrated that the interactions were static quenching.

The negative ΔG values indicated that the interaction processes were thermodynamically spontaneous (Table 1). The highest negative ΔG value in the 4-NP > 100 kDa HA system was observed at the same temperature, manifesting that >100 kDa HA possessed the largest interaction potential for 4-NP.[20] The negative ΔH values implied that the interaction processes were

exothermic, and the positive values of ΔS suggested the disorder of the reaction systems increased after 4-NP interaction with MW-fractionated HAs. Previous studies[41,42] reported that the positive ΔH and ΔS values were frequently considered as hydrophobic forces, whereas negative ΔH and ΔS values occurred for van der Waals forces and hydrogen bonding; besides, if $\Delta H < 0$ and $\Delta S > 0$, the interaction process was mainly driven by electrostatic forces. Therefore, the positive values of ΔH and ΔS observed in this study indicated that hydrophobic forces were responsible for the interactions between MW-fractionated HAs and 4-NP under the experimental condition (pH 6, 1 mM NaNO$_3$).

3.2.3. Interactions between 4-NP and MW-fractionated HAs at different pH values and ionic strengths. Ionizable organic pollutants binding to HA exhibits a strong pH-dependence, reflecting the speciation of both the sorbent and sorbate.[41,43] The binding parameters at various pH values were listed in Table S3.† The fluorescence emission spectra of the 4-NP–HAs systems at pH 3.0 and pH 11.0 were provided in Fig. S5 and S6.† The relationship of K_{HA} vs. pH was presented in Fig. 4a. At pH 3.0, the carboxyl groups of HAs were protonated, resulting
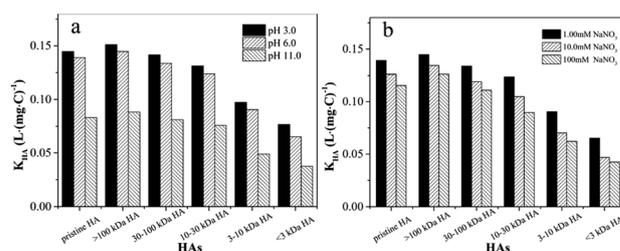

Fig. 4 Effect of pH (a) and IS (b) on 4-NP–HAs systems (Ex/Em = 280/308 nm; 298 K).

in a reduction of polarity. At the same time, protonation of HAs facilitated intra- and intermolecular interactions, leading to the formation of additional hydrophobic cavities in which more hydrophobic compounds were adsorbed.[44] With the increasing pH, the molecular would extend and uncoil due to the deprotonation of phenolic and carboxyl groups. Consequently, MW-fractionated HAs become less hydrophobic and more polar, which was unfavorable for binding of 4-NP.[45] Furthermore, with further increasing to pH 11.0, the 4-NP mainly existed as foremost ionic forms when pH was higher than pK_a (10.7). As the electronegativity of HAs also enhanced with the elevating pH, electrostatic repulsion between negative charge of HAs and 4-NP would weaken the binding strength.[28] Generally, a significant reduction of K_{HA} for low molecular weight MW-fractionated HAs was observed with increasing pH (Fig. S7a†). The different extent of decrease among HA fractions was probably attributed to their respective compositional and structural characteristics.[46] As shown in Table S2,† low molecular weight MW-fractionated HAs were more enriched in polar groups and have much higher polarity compare with other fractions. Consequently, <3 kDa HA could be easily bound *via* molecular interactions at lower pH, resulting in more sensitivity to pH.[46]

In addition, IS would affect the interactions by destroying the HA structure and compressing the double electric layers on molecule surface.[20,47] The fluorescence emission spectra of the 4-NP–HAs systems at 10 mM and 100 mM NaNO₃ were provided in Fig. S8 and S9.† Fig. 4b showed the binding constants of MW-fractionated HAs dramatically decreased with NaNO₃ concentration from 1 mmol L^{-1} to 100 mmol L^{-1} at neutral pH solution. All MW-fractionated HAs exhibited a similar trend. The high concentration ions compressed the thickness of the electric double layer of HA colloids effectively, inducing HA aggregation and even precipitation.[45,48] This tightly packed molecular shape of HA would reduce the capability of 4-NP to interact with HA.[49] Furthermore, the decrease of the K_{HA} in high molecular weight MW-fractionated HAs was smaller than that in low molecular weight MW-fractionated HAs (Fig. S7b†). The reduction of K_{HA} was mainly deemed to the change of HAs molecular size, which was caused by the associations between cations and acidic groups. Thus, the contents of negatively charged acidic functional groups of HAs were probably responsible for the different results among MW-fractionated HAs, which was consistent with the experimental results for hydrophobic fractions and different origins of DOM.[49,50]

3.3. UV-vis, FT-IR, ¹H NMR spectra of 4-NP–HAs complexations

The UV-vis absorption spectra of 4-NP in the absence and presence of MW-fractionated HAs at pH 6 and 1 mM NaNO₃ were measured and presented in Fig. 5a. With addition of equivalent MW-fractionated HAs, the absorption intensities and shapes of 4-NP changed. As the molecular weight of fractionated HAs decreased, a slight blue shift was observed for the absorption peak at around 275 nm.[20] The apparent variation indicated that steady 4-NP–HAs complexes were formed and the molecular weight of HA had a significant effect on the micro-
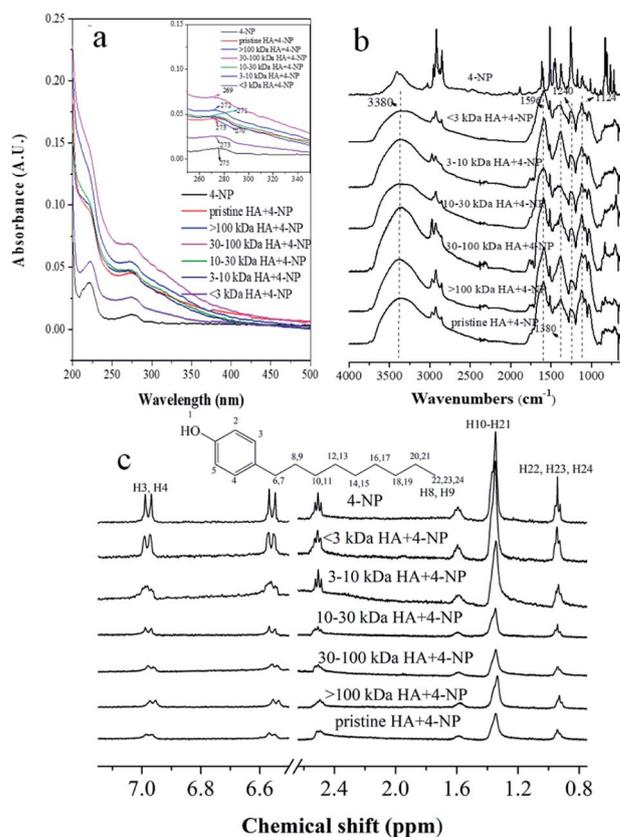

Fig. 5 UV-visible absorption (a) and FTIR (b) and ¹H NMR (c) spectra of 4-NP in the absence and presence of MW-fractionated HAs. The insert in (a) was the magnification of UV-visible absorption. Assignments were presented in the topmost spectra.

environmental changes of 4-NP. Besides, the distinct changes further confirmed that static quenching occurs in the interactions. This was because the dynamic quenching hardly affected absorption spectra of quenching matters.

To explore the changes of MW-fractionated HAs functional groups complexing with 4-NP, the FT-IR spectra of 4-NP exposed to HA at pH 6 and 1 mM NaNO₃ were collected and shown in Fig. 5b. Compared with the MW-fractionated HAs spectra, the significantly increased absorption intensity at 1380, 1240, and 1124 cm^{-1} was attributed to C–O stretching vibration, phenolic O–H, and C–H bending vibration of 4-NP, respectively.[51] The peaks of the H-bonded OH vibration moved slightly to the low wavenumber, and the peaks were broadened when exposed to HAs, implying H-bonding involving the 4-NP in HA.[20] The C=C peak of MW-fractionated HAs after binding shifted from 1635 to 1596 cm^{-1}, which could be attributed to the π–π interactions between the benzene rings of 4-NP and MW-fractionated HAs.[39,52] These features of the FTIR spectra proved that the 4-NP was not mechanically mixed with the HAs but bound to the MW-fractionated HAs.

Nuclear magnetic resonance (NMR) was applied to provide molecular-level information involved in the reactions between 4-NP and HAs. As shown in Fig. 5c, the chemical shifts above 6.2 ppm were attributed to the 4-NP protons of the aromatic

region, while the signals resonating between 1 and 4.7 ppm corresponded to protons in the aliphatic regions. Due to the lower concentration of MW-fractionated HAs, almost no proton NMR signal was observed (Fig. S10†). Upon addition of MW-fractionated HAs, the proton signals of 4-NP were quenched and broadened, suggesting a more rapid relaxation rate due to dipolar interactions arising from restricted mobility of 4-NP molecules.[20,53,54] Simultaneously, the chemical shifts of aromatic proton signals moved upfield due to the increased electron shielding around proton nuclei.[23] Though similar trends were observed in all 4-NP–HAs systems, the extent of signal changes (H3, H4 and H2, H5) was larger for high molecular weight MW-fractionated HAs than that of low molecular weight MW-fractionated HAs (Fig. S11†). These observations might be attributed to the establishment of π–π interactions between 4-NP and the aromatic parts of HAs, where the center of magnetic anisotropy was shifted out of the 4-NP aromatic plane toward the center of newly formed π–π complexes.[20,53] The strong π–π interactions would be formed between 4-NP and high molecular weight MW-fractionated HAs, leading to increasing the electron shielding of proton nuclei. In addition, the nuclei of 4-NP entrapped in higher hydrophobic cavities of >100 kDa HA might induce an improved magnetic shielding, causing a larger upfield shift.[55,56] In previous studies, the hydrogen bonding interaction was also used to explain the upfield shift between HA and aromatic organic pollutants.[20,57] However, the chemical shift variation was smaller for more hydrophilic and nonpolar MW-fractionated HAs. Therefore, the interaction between 4-NP and HAs should not be primarily related to H-bonding at high pH.[53] Overall, π–π interactions between aromatic rings of 4-NP and MW-fractionated HAs and hydrophobic interactions played important roles in the interaction process.

3.4. Relationships of the physicochemical properties with interaction properties

The varied interaction properties of MW-fractionated HAs may be related to their distinct chemical compositions and structures. As shown in Fig. 6, the log K_{HA} values are strongly positively correlated with SUVA$_{254}$ ($R^2 > 0.872$), implying that the

aromatic structures of HAs have critical importance in the interaction process of 4-NP with MW-fractionated HAs. The results were consistent with the studies of HOCs interaction with MW-fractionated HAs.[13,14,58,59] HIX was also positively correlated with the log K_{HA}. Higher values of HIX suggested higher degrees of aromaticity, lower rates of mineralization, and lower contents of oxygen-containing functional groups for DOM.[40] The importance of humification degree was highlighted in the interaction process between HOCs and DOM fractions.[14,15] Additionally, (O + N)/C atomic ratios, as an index of the polarity of HA, negatively correlated with log K_{HA} values. Similarly, Jin et al.[58] observed that HA fractions with higher polarity had lower interaction properties for phenanthrene than other HA fractions. It has been proposed that the hydrophilic moieties of HA would reduce the accessibility of HOCs to sorption domains and compete for sorption sites, thus decreasing their interactions.[60] Taken together, the superior interaction property for the high molecular weight MW-fractionated HAs resulted from its higher aromaticity, humification degree, and lower polarity.

Principal component analysis (PCA) is a multivariate statistical technique that can be used to simplify the selected parameters and convert the data into graphical form. To further understand the hetero-interaction of 4-NP with HA, PCA was performed by using the selected parameters of the HA samples (e.g., C, H, O, N, MW, Mn, HIX, SUVA$_{254}$, O/C, (N + O)/C, BIX (biological index), FI (fluorescence index), K_{HA}, K, n) that had relationships with formation of 4-NP–HAs complex. As seen in Fig. 7a, the percentage of variance of principal component 1 (PC1) and principal component 2 (PC2) was approximately 78.4% and 10.3% in the HA samples, respectively. The cumulative percentage of variance of PC1 and PC2 is 88.7%, indicating the interaction behavior mainly considered the two components of PC1 and PC2. The factors associated with aromaticity and MW were loaded mainly by PC1 and were positively related to PC1. The high statistically significant correlation among MW, Mn, HIX, SUVA$_{254}$, K_{HA} suggest that these factors are similar. In addition, the loadings graph also exhibited that K_{HA} has a strong relationship with SUVA$_{254}$, MW and HIX, confirming that aromatic C in MW-fractionated HAs
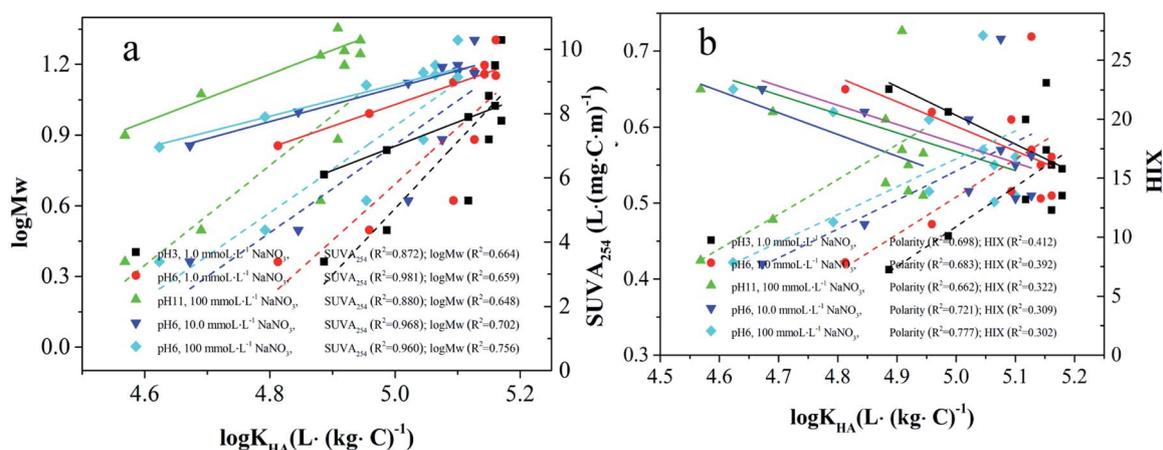

Fig. 6 Relationships of log K_{HA} with (a) SUVA$_{254}$, log MW and (b) polarity, HIX of the MW-fractionated HAs used in this study.
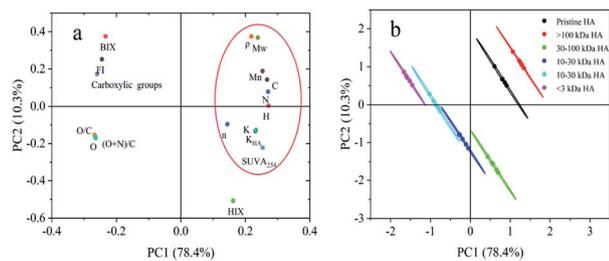
Fig. 7 (a) Factor loading plot for selected structural characteristics of MW-fractionated HAs samples as the first two principal components; (b) factor score plot for each MW-fractionated HAs sample as the first two principal components.

may significantly take part in the interactions. These results are vital for elucidating the formation of 4-NP–HAs in the future. Furthermore, in the scores graph (Fig. 7b), the distribution of different types of HA was obvious distinct, suggesting a clear interaction heterogeneity among MW-fractionated HAs sample, and proving that the critical differences in structural characteristics resulted in a difference in the 4-NP–HA complex.

3.5. Environmental implication

4-NP has been broadly distributed in aquatic environments. Thus, highly hydrophobic NPs 4-NP has inevitably interacted with ubiquitous HA in the environments. In this study, the HA samples used were environmentally related concentrations, which indicated the feasibility of extrapolating these results to natural ecosystems. Additionally, previous work about 4-NP–HA interaction mainly focused on the bulk HA samples, ignoring the effects of the heterogeneities within the bulk HA on the interaction behaviors.[10] This work highlighted MW-dependent interaction heterogeneities of HA, which suggested that heterogeneity in MW distribution should be taken into consideration when exploring the 4-NP–HA interactions and assessing the fate and transport of 4-NP in aquatic environments.

4-NP could interact with MW-fractionated HAs to form a relative stable complex spontaneously. Generally, higher molecular weight MW-fractionated HAs have stronger sorption ability to 4-NP than lower higher molecular weight MW-fractionated HAs. *Via* a correlation analysis and PCA, the results indicated that aromaticity and MW played vital roles in the interaction process. Higher MW of HA accompanied with higher aromatic moieties had prone to interaction with 4-NP, which might significantly influence the biodegradation of 4-NP. As Lin *et al.*[12] pointed out, the DOM concentration and structure, organism species, exposure regime. As well as water conditions could influence the biodegradation of pollutants. Thus, the biodegradation of MW-fractionated HAs-associated 4-NP are needed to be precisely investigated in further researches. Moreover, the formation of 4-NP–HAs complex was mainly induced by hydrophobic interactions and π–π interactions, which could be interfered by different pHs and ISs. These results herein were helpful for understanding the effects of MW distribution of HA on the interaction with 4-NP under environmentally relevant conditions.

4. Conclusions

The interaction of the MW-dependent fractionated HAs with 4-NP were explored by EEM, UV-visible spectroscopy, FT-IR, and ^{1}H NMR analysis. The quenching processes of all samples were static, and the binding affinities calculated from the Stern–Volmer and site-binding equations reduced with the MW decreased, exhibiting a clear MW-dependent binding heterogeneity in aquatic environments. The binding constants for 4-NP–HAs system were suppressed as the ionic strength decreased and pH increased. The binding reactions occurred spontaneously, and the interactions were mainly driven by hydrophobic interaction. Additionally, π–π interactions between aromatic rings of 4-NP and MW-fractionated HAs might play crucial roles in forming the 4-NP–HAs complex, as indicated by FT-IR and ^{1}H NMR. This study highlighted the importance of MW in HA interaction with 4-NP, which can influence the fate and behavior of 4-NP in aquatic environments. Besides heterogeneity, the regional and temporal variation in different sources of HA also has important impacts on the interaction, which should be further assessed for predicting the behavior of 4-NP in natural environments.

Author contributions

The manuscript was written through contributions of all authors. All authors have given approval to the final version of the manuscript.

Conflicts of interest

The authors declare no competing financial interest.

Acknowledgements

References

1 W. de Bruin, Q. Kritzinger, R. Bornman and L. Korsten, *Ecotoxicol. Environ. Saf.*, 2019, **181**, 419–427.

2 K. Vargas-Berrones, L. Bernal-Jacome, L. Diaz de Leon-Martinez and R. Flores-Ramirez, *Sci. Total Environ.*, 2020, **726**, 138493.

3 G. Bhandari, A. R. Bagheri, P. Bhatt and M. Bilal, *Chemosphere*, 2021, **275**, 130013.

4 Y. Hu, W. Wu, D. Xu, X. Guan and S. Wang, *J. Hazard. Mater.*, 2021, **406**, 124773.

5 Y. Hong, C. Feng, Z. Yan, Y. Wang, D. Liu, W. Liao and Y. Bai, *Environ. Chem. Lett.*, 2020, **18**, 2095–2106.

6 Z. Noorimotlagh, S. A. Mirzaee, S. S. Martinez, D. Rachon, M. Hoseinzadeh and N. Jaafarzadeh, *Environ. Res.*, 2020, **184**, 109263.

7 W. Limmun, N. Ishikawa, J. Momotori, M. Terasaki, T. Sato, K. Kikuchi, M. Sasamoto, T. Umita and A. Ito, *Environ. Sci. Pollut. Res. Int.*, 2022, **29**, 18882–18890.

8 X. Liao, C. Zhang, L. Yao, J. Li, M. Liu, L. Xu and M. Evalde, *Sci. Total Environ.*, 2014, **473–474**, 530–536.

9 Z. Jin, X. Wang, Y. Sun, Y. Ai and X. Wang, *Environ. Sci. Technol.*, 2015, **49**, 9168–9175.

10 C. Li, A. E. Berns, A. Schäffer, J.-M. Séquaris, H. Vereecken, R. Ji and E. Klumpp, *Chemosphere*, 2011, **84**, 409–414.

11 S. Rizzuto, K. C. Jones, H. Zhang, D. L. Baho, E. Leu and L. Nizzetto, *Chemosphere*, 2021, **285**, 131524.

12 H. Lin, X. Xia, S. Bi, X. Jiang, H. Wang, Y. Zhai and W. Wen, *Environ. Sci. Technol.*, 2018, **52**, 644–653.

13 M. S. Shi, W. S. Huang, L. F. Hsu, Y. L. Yeh and T. C. Chen, *Int. J. Environ. Res. Public Health*, 2019, **16**, 5087.

14 Y. K. Lee, M. H. Lee and J. Hur, *Sci. Total Environ.*, 2019, **660**, 169–176.

15 Y. L. Yeh, K. J. Yeh, L. F. Hsu, W. C. Yu, M. H. Lee and T. C. Chen, *J. Hazard. Mater.*, 2014, **277**, 27–33.

16 C. W. Chuang, W. S. Huang, H. S. Chen, L. F. Hsu, Y. Y. Liu and T. C. Chen, *Int. J. Environ. Res. Public Health*, 2021, **18**, 1102.

17 K. N. McPhedran, R. Seth and K. G. Drouillard, *Environ. Sci. Technol.*, 2013, **47**, 2548–2553.

18 L. Bai, Z. Zhao, C. Wang, C. Wang, X. Liu and H. Jiang, *Chemosphere*, 2017, **187**, 421–429.

19 S. Greish, A. Rinnan, H. Marcussen, P. E. Holm and J. H. Christensen, *Environ. Sci. Pollut. Res. Int.*, 2018, **25**, 299–311.

20 X. Zhao, Z. Hu, X. Yang, X. Cai, Z. Wang and X. Xie, *Environ. Pollut.*, 2019, **248**, 815–822.

21 W. Chen, P. Westerhoff, J. A. Leenheer and K. Booksh, *Environ. Sci. Technol.*, 2003, **37**, 5701–5710.

22 H. Ren, F. Ma, X. Yao, K. Shao and L. Yang, *J. Hydrol.*, 2020, **591**, 125289.

23 B. Chaubey, P. Narwal, A. Khandelwal and S. Pal, *J. Photochem. Photobiol., A*, 2021, **405**, 112986.

24 S. Yao, M. Fabbricino, L. Pontoni, M. Race, F. Parrino, L. Savignano, G. D'Errico and Y. Chen, *Chemosphere*, 2021, **286**, 131528.

25 Y. Yin, M. Shen, Z. Tan, S. Yu, J. Liu and G. Jiang, *Environ. Sci. Technol.*, 2015, **49**, 6581–6589.

26 A. Hafuka, Q. Ding, H. Yamamura, K. Yamada and H. Satoh, *Water Res.*, 2015, **85**, 193–198.

27 B. Benmansour, L. Stephan, J. Y. Cabon, L. Deschamps and P. Giamarchi, *J. Fluoresc.*, 2011, **21**, 843–850.

28 Z. R. Yan, H. S. Meng, X. Y. Yang, Y. Y. Zhu, X. Y. Li, J. Xu and G. P. Sheng, *J. Environ. Manage.*, 2019, **232**, 219–225.

29 M. H. Shen, Y. G. Yin, A. Booth and J. F. Liu, *Water Res.*, 2015, **71**, 11–20.

30 K. Yang, G. Miao, W. Wu, D. Lin, B. Pan, F. Wu and B. Xing, *Chemosphere*, 2015, **138**, 657–663.

31 Z. Zhang, C. Lü, J. He, M. Gao, B. Zhao, B. Zhou, J. Guo, H. Zhou, X. Liu, Z. Li, W. Shi, Y. Jiao, W. Zhao and Y. Zhang, *Chemosphere*, 2018, **191**, 458–466.

32 J. Yang, P. Xu, L. Hu, G. Zeng, A. Chen, K. He, Z. Huang, H. Yi, L. Qin and J. Wan, *Environ. Sci.: Nano*, 2018, **5**, 2699–2711.

33 J. Ren, W. Fan, X. Wang, Q. Ma, X. Li, Z. Xu and C. Wei, *Water Res.*, 2017, **108**, 68–77.

34 F. C. Wu, R. D. Evans and P. J. Dillon, *Environ. Sci. Technol.*, 2003, **37**, 3687–3693.

35 J. Chen, B. Gu, E. J. Leboeuf, H. Pan and S. Dai, *Chemosphere*, 2002, **48**, 59–68.

36 J. Chen, E. J. Leboeuf, S. Dai and B. Gu, *Chemosphere*, 2003, **50**, 639–647.

37 H. Bai, Z. Jiang, M. He, B. Ye and S. Wei, *J. Environ. Sci.*, 2017, **154**, 165.

38 L. Wang, H. Li, Y. Yang, D. Zhang, M. Wu, B. Pan and B. Xing, *Water Res.*, 2017, **122**, 337–344.

39 D. Ren, B. Huang, B. Yang, X. Pan and D. D. Dionysiou, *J. Hazard. Mater.*, 2017, **327**, 197–205.

40 J. Hur, M.-H. Park and M. A. Schlautman, *Environ. Sci. Technol.*, 2009, **43**, 2315–2321.

41 Z. Zhang, M. Yang, J. Yi, Q. Zhu, C. Huang, Y. Chen, J. Li, B. Yang and X. Zhao, *ACS Omega*, 2019, **4**, 563–572.

42 Z. Akdogan and B. Guven, *Environ. Pollut.*, 2019, **254**, 113011.

43 I. Christl, M. Ruiz, J. R. Schmidt and J. A. Pedersen, *Environ. Sci. Technol.*, 2016, **50**, 9933–9942.

44 R. Wang, S. Yang, J. Fang, Z. Wang, Y. Chen, D. Zhang and C. Yang, *Int. J. Environ. Res. Public Health*, 2018, **15**, 1458.

45 B. Pan, S. Ghosh and B. Xing, *Environ. Sci. Technol.*, 2008, **42**, 1594–1599.

46 Y. Mei, Y. Bai and L. Wang, *Acta Geochim.*, 2016, **35**, 288–293.

47 C.-L. Lee, L.-J. Kuo, H.-L. Wang and P.-C. Hsieh, *Water Res.*, 2003, **37**, 4250–4258.

48 K.-C. Chang, C.-L. Lee, P.-C. Hsieh, P. Brimblecombe and S.-M. Kao, *Environ. Sci. Pollut. Res.*, 2015, **22**, 13234–13242.

49 L.-J. Kuo and C.-L. Lee, *Environ. Toxicol. Chem.*, 2005, **24**, 886–894.

50 T. Polubesova, M. Sherman-Nakache and B. Chefetz, *Environ. Sci. Technol.*, 2007, **41**, 5389–5394.

51 C. Song, X. F. Sun, S. F. Xing, P. F. Xia, Y. J. Shi and S. G. Wang, *Environ. Sci. Pollut. Res. Int.*, 2014, **21**, 1786–1795.

52 T. Li, Y. He and X. Peng, *Chemosphere*, 2020, **251**, 126370.

53 D. Šmejkalová and A. Piccolo, *Environ. Sci. Technol.*, 2008, **42**, 8440–8445.

54 M. Bedard, K. A. Giffear, L. Ponton, K. D. Sienerth and V. Del Gaizo Moore, *Biophys. Chem.*, 2014, **189**, 1–7.

55 J. Xu, Y. Y. Hu, X. Y. Li, J. J. Chen and G. P. Sheng, *Environ. Pollut.*, 2018, **243**, 752–757.

56 P. Mazzei and A. Piccolo, *Environ. Sci. Technol.*, 2012, **46**, 5939–5946.

57 W. Fang, G.-P. Sheng, L.-F. Wang, X.-D. Ye and H.-Q. Yu, *Environ. Pollut.*, 2015, **207**, 123–129.

58 J. Jin, K. Sun, Y. Yang, Z. Wang, L. Han, X. Wang, F. Wu and B. Xing, *Environ. Sci. Technol.*, 2018, **52**, 1880–1888.

59 X. M. Chen, Y. Zhao, Y. Y. Ma, L. J. Zhu, T. X. Yang, Z. M. Wei, Y. L. Dong and Q. B. Wei, *Ecotoxicol. Environ. Saf.*, 2018, **147**, 394–400.

60 X. Wang, X. Guo, Y. Yang, S. Tao and B. Xing, *Environ. Sci. Technol.*, 2011, **45**, 2124–2130.